Properties of high-Tc superconductors at RF and microwaves : experimental data and some model notions

O.G. Vendik, A.B. Kozyrev, A. Yu. Popov

Tome 25 N° 3 MARS 1990

REVUE DE PHYSIQUE APPLIQUÉE

Revue Phys. Appl. **25** (1990) 255-263 MARS **1990,** PAGE 255

Classification
Physics Abstracts
74.30 — 74.30G — 74.70V

Properties of high-T_c superconductors at RF and microwaves : experimental data and some model notions

O. G. Vendik, A. B. Kozyrev and A. Yu. Popov

Department of Physical Electronics, V. I. Ulyanov (Lenin) Institute of Electrical Engineering, 197022 Leningrad, U.S.S.R.

(*Reçu le 16 mars 1989, révisé le 3 novembre 1989, accepté le 28 novembre 1989*)

Résumé. — Nous tentons dans cet article de résumer le comportement expérimental obtenu à ce jour des supraconducteurs à haute température critique (SHTC) dans les domaines rf et micro-onde. La majeure partie de notre étude se rapporte à l'YBaCuO pour lequel les données expérimentales sont les plus nombreuses. Nous démontrons que les jonctions intergranulaires jouent un rôle essentiel pour les propriétés électromagnétiques des céramiques dont la résistivité est de l'ordre de $\rho \approx 1\,000\ \Omega \times \text{cm}$. Nous proposons un modèle pour les monocristaux de SHTC où les porteurs de charges sont des « bi-trous » localisés au sein d'une cellule élémentaire obéissant à la statistique de Bose et agissant par effet tunnel. Ce modèle peut décrire les évolutions en température de la profondeur de pénétration du champ et de la densité de courant critique ainsi que les évolutions en température et fréquence de la résistance de surface. La présence de régions normales localisées aux macles entre des domaines supraconducteurs peut être la cause de la résistance résiduelle observée dans les monocristaux de SHTC. Les résultats expérimentaux sont en bon accord avec les déductions de nos modèles.

Abstract. — In this paper we try to summarize experimental data on high-T_c superconductors (HTSC) behaviour in RF and microwave electromagnetic field accumulated to this day. The main emphasis is made on Y-Ba-Cu-O material for which the most complete information is available. We show that it is intergranular junctions that play an essential role in the formation of electromagnetic properties of the ceramics with $\rho \cong 10^{-4}\ \Omega \times \text{m}$. We suggest a model of the HTSC single crystal where the charge carriers are tunneling « biholes » obeying the Bose statistics and are localized within a unit cell. This model can describe field penetration depth and critical current density as a functions of temperature as well as temperature and frequency dependence of surface resistance. The presence of normal conducting regions can be a course of HTSC single crystal residual resistance. A close agreement between experimental data and model calculations is demonstrated.

1. Introduction.

The discovery of high-T_c superconductivity (HTSC) in res o pro ems in the field of superconductive physical phenomena and to searching the ways of practical implementation of superconductors in electronic and electrical engineering devices which could operate at liquid nitrogen temperature.

The first steps in generalization of the physical information available and in predictions of practical applications have been attempted [1, 2]. The perspectives of applications of high-T_c superconductors in electronics [3] and especially in microwave electronics [4, 5] are of great interest. The solution of applied problems in microwave electronics may constitute the closest perspective for practical realizations of vast possibilities of HTSC.

t seems to us not unfounded to state that the epitaxial structurally perfect films of HTSC can become the basis for practical use as elements of microwave devices [3-5]. On the other hand, the investigations of films provide rich information about the nature of HTSC phenomena which is highly important in solving purely physical problems. It is crucial to improve the HTSC single crystal technology because such single crystals are indispensable with in physical studies and because they can form the basis for new elements of HTSC electronics.

At present there is no complete theoretical de-

scription of HTSC phenomena at microscopic level. However, this fact does not exclude construction of phenomenological models giving quantitative descriptions of HTSC materials' properties. It is convenient to distinguish the following characteristics of these materials : resistivity ρ, RF and microwave surface resistance R_s, and critical current density j_c. It is necessary to study how these characteristics depend on temperature, frequency of electromagnetic field and strength of constant and/or alternating magnetic fields. The most important quantitative characteristic of the material is the field penetration depth. Three different cases should be distinguished at analysis of experimental data and development of model notions : 1) granular materials (ceramics or polycrystalline films), 2) single crystals with twinned domains, and 3) homogeneous crystals. The very first experimental data have been obtained on ceramic samples. Therefore it would be convenient first of all to consider the properties of these samples in which the intergranular contacts play the major role. Then we consider the single crystal properties and after that influence of twin domains on these properties. The existence of twin domains in single crystal can probably result in residual resistance and lowering of the critical current density.

2. Experimental data on electrophysical parameters of HTSC materials.

The complex oxide $YBa_2Cu_3O_{7-x}$ is a typical HTSC material. It is highly anisotropic which manifests itself in difference of electrical characteristics measured along *c*-axis or in *ab*-plane. In the following we shall consider currents confined in the *ab*-plane only, the transport processes along the *c*-axis being excluded from the consideration.

Important parameters of both bulk and film materials are critical temperature T_c, temperature width of transition ΔT_c, and resistivity just above the critical temperature $\rho(T_c)$. For single crystals and structurally perfect films of $YBa_2Cu_3O_{7-x}$ these are : T_c = 90-93 K, ΔT_c = 0.5-1.5 K, $\rho(T_c)$ = (0.4-1.5) 10^{-6} $\Omega \times$ m. The measure of nonstoichiometry in oxygen further denoted x plays an essential role with the best results for x = 0.0-0.2.

Critical current density heavily dependends on the structural quality of the film. Typical j_c values are : 10^{10} A/m^2 at 78 K and up to 10^{11} A/m^2 at 4.2 K [6-10]. The known theoretical estimates [3] show that a material with perfect structure should have j_c value of about 10^{13} A/m^2 near T = 0.

Some properties of multicomponent oxides like Bi-Sr-Ca-Cu-O with $T_c \geqslant 100$ K are reported in recent publications [11]. Epitaxial films of this compound exist [12], as well as compounds with Bi partially substituted by Pb [13]. The complex oxides Tl-Ba-Ca-Cu-O with $T_c \cong 120$ K [14, 15] are of considerable interest. The profit of practical applications of materials with $T_c \cong$ 120-150 K is obvious. The operation temperature set by boiling nytrogen equals to 78 K, i.e. (0.5-0.7) T_c, which ensures the stability of material parameters with respect to temperature and transport current density fluctuations. In spite of these attractive features we shall devote this review to another material, namely Y-Ba-Cu-O, since the corresponding technology is most advances and the quantitative characteristics obtained are most reliable.

As mentioned above, an important parameter of HTSC film is its RF and microwave surface resistance R_s. Figure 1 summarizes experimental data taken from numerous references [16-25]. Figure 2 shows the experimental dependences of R_s on T for three different materials obtained at the frequencies 60 GHz (curves marked with 1) and 37 MHz (curves marked with 2). The results of R_s measurements in the coarse-grained ceramics Y-Ba-Cu-O with ρ (100 K) $\approx 10^{-4}$ $\Omega \times$ m [26] are presented in figure 2a. Figure 2b shows R_s *versus* T plot for high quality Y-Ba-Cu-O ceramics (ρ (100 K) $\approx$ 10^{-6} $\Omega \times$ m) with smaller grains as compared to the previous case. This sample has been fabricated by cryochemical technology [16]. The results of R_s measurements for Ho-Ba-Cu-O epitaxial film (ρ (100 K) = 7×10^{-7} $\Omega \times$ m) on the $SrTiO_3$ (001) substrate are shown in figure 2c [17, 23].

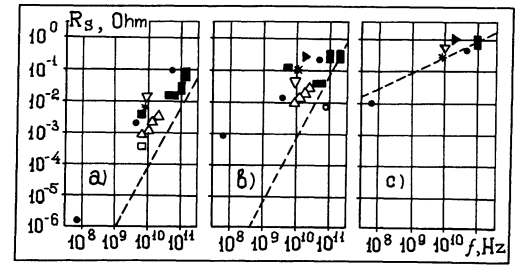

Fig. 1. — Frequency dependence of HTSC materials surface resistance R_s for T = 4.2 (a), 78 (b), 300 K (c). The dashed line corresponds to the model calculations. Experimental data are taken from : (●) [16], (▶) [17], (▽) [18], (□) [19], (*) [20], (○) [21], (■) [22], (▬) [23], (▮) [24], (△) [25].

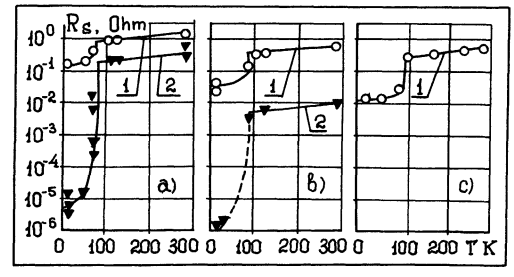

Fig. 2. — Temperature dependence of coarse-grained Y-Ba-Cu-O (a), high quality Y-Ba-Cu-O (b), and epitaxial Ho-Ba-Cu-O film (c) surface resistance R_s at frequencies 60 GHz (1) and 37 MHz (2).

Consider some model ideas which make it possible to relate R_s frequency and temperature dependences to structural features of crystals used in experiments.

3. Model of surface resistance formation in HTSC ceramics.

From macroscopic electrodynamics point of view HTSC ceramics can be treated as a system of grains connected by Josephson-like junctions of S-N-S type. This structure has been realized at an early stage of investigations [26, 28]. This picture is confirmed by numerical estimates of ceramics [28] and polycrystalline films parameters [29] and forms the basis for a phenomenological model [30].

The model is illustrated in figure 3a. It presents a surface of ceramic sample visible from the incident wave direction. Suppose the granular size d to be negligible as compared to the vacuum wavelength. To describe the field penetration into the sample we imagine a wave-guide restricted by electrical ($\mathbf{E}_\tau = 0$) and magnetic ($\mathbf{H}_\tau = 0$) walls. The cross section of the wave-guide is marked with dotted line in figure 3a. Further, figure 3b shows a chain of conjucted spheres along which the vertically polarized electromagnetic wave penetrates into the sample. The above mentioned wave-guide can be represented by fragments of a transmission line loaded by lumped impedances. The equivalent circuit of the spheres-junction periodic structure is presented in figure 3c. We assume the intrinsic resistance of spherical grains to be negligible as compared to the resistance of junction R_N. Moreover, later on we neglect the inductance of the grain L_0.

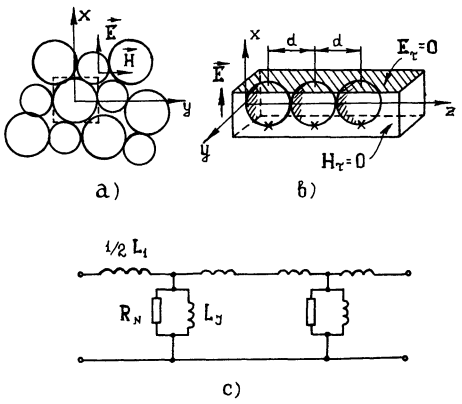

Fig. 3. — The system of perfectly conducting spheres connected by junctions (a), chain of spheres with their junctions (b). E is an electric component vector of incident electromagnetic wave. Equivalent circuit of spheres-junctions periodic structure (c).

The whole of sample surface could be divided into waveguides in accordance with our procedure. In practice grains are of random size. Methods of technical electrodynamics enable us to calculate parameters of the wave-guide system with statistical characteristics. Our calculation will be restricted by regular structure with averaged parameters. To our knowledge such a simulation gives reliable results.

If the dc resistivity of the sample for $T > T_c$ is known then resistance of an isolated junction is

$$R_N = \rho / d \,. \tag{1}$$

The critical current I_c can be expressed through the critical current density that destroys the superconductivity of the intergranular junctions :

$$I_c = j_c \, d^2 \,. \tag{2}$$

The I_c value defines the inductance of the Josephson-like junction for $I < I_c$ [31] :

$$L_J = \frac{\Phi_0}{2 \pi I_c} \tag{3}$$

where $\Phi = h/2e$ is a flux quantum.

The transmission line inductance between spheres is

$$L_1 = \mu_0 \, d \,. \tag{4}$$

Thus, the impedance and conductance of the unity length of the equivalent transmission line is given by

$$Z_1 = i \omega \mu_0, \quad Y_1 = [R_N^{-1} - i (\omega L_J)^{-1}] \, d^{-1} \,. \tag{5}$$

Now it is easy to find the expression for the surface impedance and the propagation constant of the structure :

$$Z_s = \sqrt{(1 + (d\gamma/2)^2) \, Z_1 / Y_1} \,, \quad \gamma = \sqrt{Z_1 \, Y_1} \,. \tag{6}$$

Inserting (1)-(5) into (6) we get

$$Z_s = i \omega \mu_0 \, \delta \, \sqrt{1 + (d/2\,\delta)^2} \,, \tag{7}$$

where

$$\delta = \gamma^{-1} = (\lambda_{sc}^{-2} + 2 i \delta_{sk}^{-2})^{-1/2} \,, \tag{8}$$

$$\lambda_{sc} = \frac{\Phi_0 \, d}{2 \pi I_c(T)} \,, \qquad \delta_{sk} = \sqrt{2 \rho (T) / \omega \mu_0} \,, \tag{9}$$

In the case $\delta \gg d$ we have from (7) $Z_s = i \omega \mu_0 \, \delta$. This expression is identical to one obtained for homogeneous superconductor [32]. Thus the granular medium in this case reacts to the electromagnetic wave as a homogeneous material with London penetration depth λ_{sc} and skin penetration depth δ_{sk} due to normal excitations.

Assuming different relationships between characteristic lengths d, λ_{sc} and δ_{sk} we find from (7)

$$Z_s = (1+i)\sqrt{\omega\mu_0\rho(T)/2}\,, \qquad d \ll \delta_{sk} \ll \lambda_{sc}\,, \tag{10}$$

$$Z_s = R_N + i\omega\mu_0 d/2\,, \qquad \delta_{sk} \ll d, \lambda_{sc}\,, \tag{11}$$

$$Z_s = \frac{(\omega\mu_0)^2}{\rho(T)}\frac{\lambda_{sc}^4}{d} + i\omega\mu_0 d/2\,, \qquad \lambda_{sc} \ll \delta_{sk}, d\,, \tag{12}$$

$$Z_s = \frac{(\omega\mu_0)^2}{2\rho(T)}\lambda_{sc}^3 + i\omega\mu_0\lambda_{sc}\,, \qquad d \ll \lambda_{sc} \ll \delta_{sk}\,. \tag{13}$$

Expressions (10), (11) are appropriate to both normal ($T > T_c$) and superconducting ($T < T_c$) states. In the former case (10) corresponds to normal skin-effect while (11) shows that the first layer of spheres does reflect the incident electromagnetic wave. Thus, the surface resistance of the granular structure with large grains $d \gg \delta_{sk}$ and normal state junctions is independent of frequency. It is this circumstance that distinguish the granular structure from a normal metal for which $R_s \sim \omega^{1/2}$.

Figure 4 presents frequency dependences of R_s calculated in the framework of the model under consideration for different temperatures. Figures 4a-b relate to coarse grained (CG) and high quality (HQ) Y-Ba-Cu-O ceramics, respectively. Parameters of the model d, $R_N(T)$, $I_c(T)$ which ensure the best fit to experimental data [23, 26] are given in the table below. From the equation (1) and data of the table we find $\rho(100\text{ K}) = 1.2 \times 10^{-4}\ \Omega \times \text{m}$ for CG ceramics and $\rho(100\text{ K}) = 8 \times 10^{-7}\ \Omega \times \text{m}$ for HQ ceramics. These values are in agreement with the results of dc measurements while d is close to typical granular size seen at microphotographs of ceramic samples.

	CG ceramics			HQ ceramics		
T, K	R_N, Ω	I_c, μA	d, μm	R_N, Ω	I_c, μA	d, μm
100	1.38	0	86.8	0.92	0	0.84
78	0.46	1.78		0.20	1.3	
4.2	0.14	268		0.06	643	

In order to obtain temperature dependence of surface resistance R_s we need temperature dependences of $I_c(T)$ and $R_N(T)$. We assume plausible functional forms :

$$I_c(T) = I_c(0)(1 - (T/T_c)^a)^b\,, \tag{14}$$

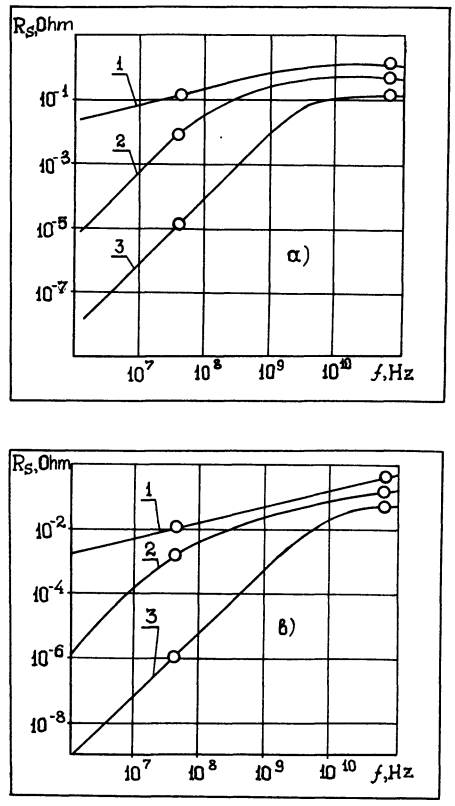

Fig. 4. — Frequency dependences of R_s for CG (a) and HQ (b) ceramic samples at $T = 100$ (1), 77 (2) and 4.2 K (3). Experimental data are taken from [23, 26].

$$R_N(T) = \begin{cases} R_0 + R_1 \exp(-\Delta(T)/kT)\,, & T < T_c \\ AT + B\,, & T > T_c \end{cases} \tag{15}$$

where $\Delta(T) = \Delta(0)(1 - (T/T_c)^{b_1})^{c_1}$,

$$A = \frac{R_N(100)}{200}(\gamma - 1)\,,$$

$$B = \frac{R_N(100)}{2}(3 - \gamma)\,, \quad \gamma = \rho(300)/\rho(100)\,.$$

Then we fix the parameters a, b, b_1, c_1 from frequency dependence of R_s.

According to dc measurements $\gamma = 1.3$ and 1.5 for CG and HQ ceramics respectively, $T_c \approx 90$ K for both samples. Using data from the table we find for CG ceramics $a = 2.44$, $b = 4.1$, $I_c(0) = 2.7 \times 10^{-4}$ A, $\Delta(0)/kT_c = 2.38$, $b_1 = 3.6$, $c_1 = 0.79$ and for HQ ceramics $a = 2.41$, $b = 4.85$, $I_c(0) = 6.45 \times 10^{-4}$ A, $\Delta(0)/kT_c = 3.05$, $b_1 = 3.86$, $c_1 = 0.77$. Figure 5 shows $I_c(T)$ and $R_N(T)$ dependences obtained. Figure 6 demonstrates a close agreement between experimental data [23, 26] and results of calculations according to formulas (7)-(9), (14), (15).

Thus, despite the obvious simplifications the model of granular medium constructed as a system of perfectly conducting grains connected by

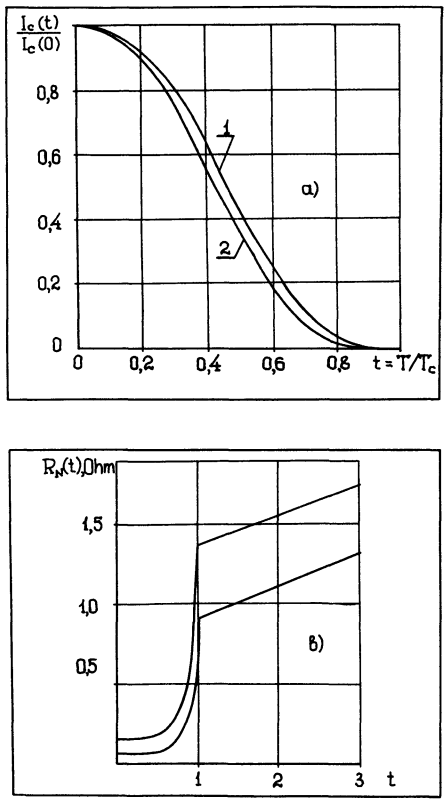

Fig. 5. — Temperature dependences of $I_c(T)$ (a) and $R_N(T)$ (b) for CG (1) and HQ (2) ceramics.

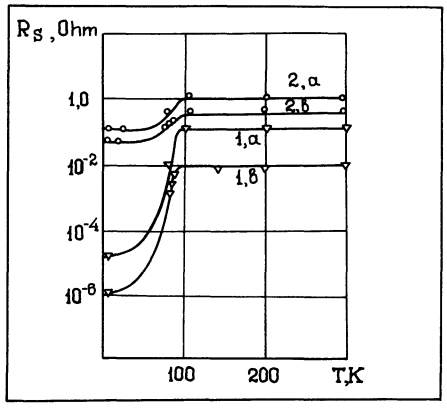

Fig. 6. — Theoretical dependences $R_s(T)$ at frequencies 37 MHz (1) and 60 GHz (2) for CG (a) and HQ (b) ceramics. Experimental data are taken from [23, 26].

Josephson-like junctions of S-N-S- type [30] adequatly describes the electrodynamic properties of HCTS ceramics.

4. A phenomenological model of HTSC single crystal.

An experimental dependence of R_s on T for the Ho-Ba-Cu-O film measured at 60 GHz [23] is presented in figure 2c. In the region $T > T_c$ $R_s(T)$ is linear function of temperature with resistivity ρ (100 K) = $7 \times 10^{-7}\ \Omega \times$ m. For T just below T_c, R_s abruptly falls to a practically constant value corresponding to the residual resistance which is typical for highly defective superconductors.

To quantitatively describe the influence of frequency and temperature on R_s we shall consider a phenomenological model based on the following ideas [33] :

a) HTSC charge carriers are localized within one lattice cell. It corresponds to the charge carriers radius coherence length of about 2-15 Å [1-3] ;

b) HTSC carriers have charge $2e$. Their behaviour is governed by Bose statistics and whenever $T < T_c$ the Bose condensation occurs. This picture is confirmed by the bipolaron superconductor model [34], by the spinbag model [35] and by the coupled-spin-mobile-hole model [36]. The models just mentioned account for the « bihole » nature of Bose charge carriers ;

c) The charge transport is caused by tunneling between adjacent cells. Particles belonging to the Bose condensate Josephson-tunnel without any potential difference. Particles out of the Bose condensate form the normal current governed by the Ohm law.

So for the whole current we can write

$$I = I_c \sin \varphi + U/R_N , \tag{16}$$

where I_c is a critical tunneling current between adjacent cells, φ is the phase difference in the Ginzburg-Landau wave function, and R_N is the resistance to the normal current.

The two adjacent cells are sketched in figure 7. Their linear dimensions correspond to the crystallographic structure of Y-Ba-Cu-O [37] : $a = 3.8$ Å, $b = 3.9$ Å, $c = 11.6$ Å. A simple geometrical consideration gives :

$$\begin{aligned} I_c &= j_c\, bc , \\ R_N &= \rho a/(bc) , \end{aligned} \tag{17}$$

where j_c is the critical current density characteristic of the material and ρ is its resistivity.

The ac charge carriers tunneling can be described by an equivalent circuit shown in figure 7, where the

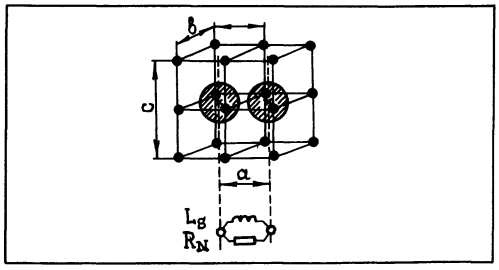

Fig. 7. — Two adjacent cells and the corresponding equivalent circuit. For definition of R_N, L_s see the text.

inductance is defined by the equation (3). Once L_S and R_N are known we can write the complex conductivity of the medium as follows :

$$\sigma_c = [R_N^{-1} - i(\omega L_S)^{-1}]\, a/(bc)\,. \qquad (18)$$

Using propositions of conducting medium electrodynamics we get

$$Z_s = \sqrt{i\omega\mu_0/\sigma_c}\,, \qquad \gamma = \sqrt{i\omega\mu_0\sigma_c}\,.$$

Further we find the penetration depth and surface resistance of the form

$$\lambda = \sqrt{\frac{\Phi_0 bc}{2\pi I_c \mu_0 a}}\,, \qquad (19)$$

$$R_s = \frac{1}{2}(\omega\mu_0)^2 \lambda^3 \rho^{-1}\,. \qquad (20)$$

In these expressions the film thickness h is greater than (2-3) λ. In the opposite case, when $h \ll \lambda$ we have

$$R_s = (\omega\mu_0)^2 \frac{\lambda^4}{h}\rho^{-1}\,. \qquad (21)$$

To use relations obtained for quantitative estimates we have to suggest temperature dependences of I_c and R_N. If « biholes » in the HTSC materials for $T < T_c$ obey the ideal Bose condensation law then

$$I_c(t) = I_c(0)(1 - t^{3/2})\,, \qquad (22)$$

$$\lambda^2(t) = \lambda^2(0)(1 - t^{3/2})^{-1}\,, \qquad (23)$$

where $t = T/T_c$ and T_c is the transition temperature. The last equation can be recast in more a convenient form :

$$\left[\frac{\lambda(t)}{\lambda(0)}\right]^{-2} = 1 - t^{3/2}\,. \qquad (24)$$

Figure 8 demonstrates the experimental curves $\lambda(t)$ obtained by different research groups [38, 39]. The solid line on the plot is in accordance with expression (24) which describes the ideal Bose condensation law. The similar dependence has been obtained theoretically in [40] with the right hand side of (24) modified by a factor which only slightly deviates from unity. The authors of paper [40] point out an acceptable agreement between their results and experimental data. We would think these facts are sufficient to justify application of the ideal Bose gas model.

To get quantitative estimates from formula (20) we need to know the function $\rho(t)$ for $t < 1$. According to the Drude-Lorentz theory

$$[\rho(t)]^{-1} = \frac{q^2 n(t)}{m_{eff}}\tau(t)\,, \qquad (25)$$

where m_{eff} is an effective mass of charge carrier, q its charge, $n(t)$ is concentration of carriers, and $\tau(t)$ is a mean free time. The concentration of particles exited from Bose condensate is given by

$$n(t) = n(1)\begin{cases} 1 & t \geqslant 1 \\ t^{3/2} & t < 1\,. \end{cases} \qquad (26)$$

An experiment [41] shows that for $t > 1$ $\rho(t) = \rho(1)\,t$. It follows from (25) that $\tau(t) = \tau(1)\,t^{-1}$ for $t > 1$. Let it be valid also for $t < 1$. Then

$$[\rho(t)]^{-1} = [\rho(1)]^{-1}\begin{cases} t^{-1} & t \geqslant 1 \\ t^{1/2} & t < 1\,. \end{cases} \qquad (27)$$

Substitution of (22), (23), (27) and (20) yields

$$R_s = \frac{1}{2}(\omega\mu_0)^2 \lambda^3(0)[\rho(1)]^{-1} t^{1/2}[f(t)]^{-3/2}\,, \qquad (28)$$

where

$$\lambda(0) = \sqrt{\frac{\Phi_0}{2\pi j_c(0)\mu_0 a}}\,, \quad f(t) = 1 - t^{3/2}\,, \qquad (29)$$

$\rho(1)$ is resistivity just above T_c, $j_c(0)$ is critical current density for $T \to 0$.

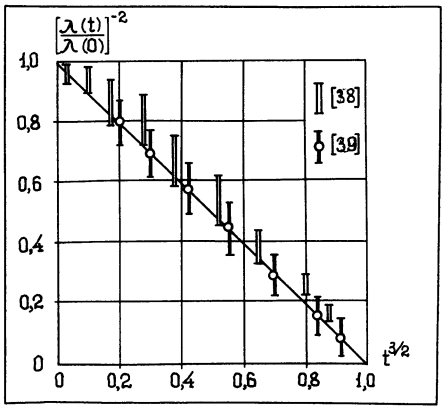

Fig. 8. — Experimental temperature dependence of magnetic field penetration depth λ. The solid line corresponds to Bose condensation law.

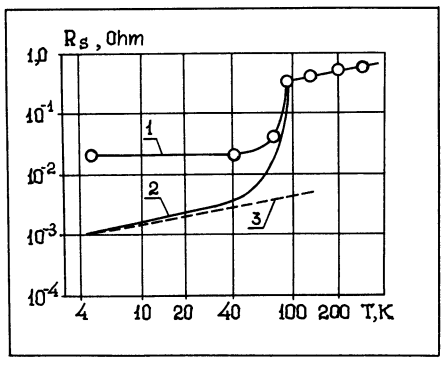

Fig. 9. — Temperature dependence of Ho-Ba-Cu-O epitaxial film surface resistance at 60 GHz : experimental data [23] (1), by expression (28) (2), an asymptotical behaviour at $T \ll T_c$ (3).

Figure 9 shows experimental values of R_s as a function of T at 60 Ghz [23] as well as the results of calculations by the expression (28) at the same frequency for $\lambda(0) = 3 \times 10^{-7}$ m and $\rho(1) = 10^{-6}\ \Omega \times$ m. The dashed line corresponds to $R_s(t) \sim t^{1/2}$ and is asymptotical to the R_s behaviour for $T \ll T_c$. A cursory inspection of figure 9 shows that instead of approaching this assymptotics the experimental curve turns into a straight line corresponding to the comparatively large residual resistance.

5. A model of the HTSC single crystal film residual resistance.

The residual resistance R_{res} of a superconductor for $T \to 0$ is due to electrons occupying quantum states which correspond to normal conductivity. Any superconductor has an ac residual resistance. The existence of sufficiently large R_{res} in HTCS materials is reported by a number research groups [28, 42].

If the residual resistance is caused by impurities and structural defects it can be eliminated through a more perfect technology. However one can encounter a situation when the normal conducting regions in a superconductor are inherent to its intrinsic properties. If this is the case the reduction of the residual resistance is of paramount importance. This part of the residual resistance in HTSC single crystal film can be caused by twinned domains in Y-Ba-Cu-O structure or, more precisely, by domain walls with normal conductivity while the bulk of the domains themselves is in a superconducting state.

Figure 10a exemplifies the structure of the twin boundary [43]. The figure shows the arrangement of Cu and O atoms at the bottom of Y-Ba-Cu-O unit cell [37]. The Cu and O atoms within two neighbouring twin blocks are situated so that the a and b axes turn out to be interchanged. In the tetragonal phase there is no stress on the twin boundary

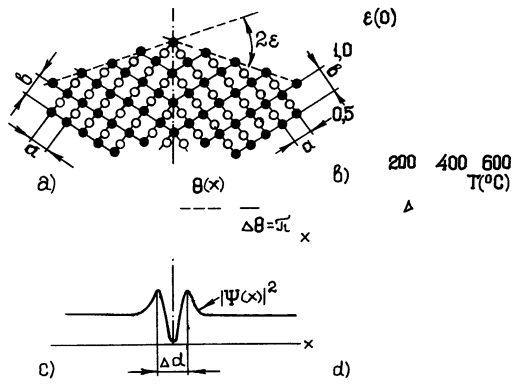

Fig. 10. — Twin domain boundary structure (a), temperature dependence of the rotation angle ε (b), Ginzburg-Landau wave function amplitude $|\psi(x)|$ and phase $\theta(x)$ behaviour at the boundary (c), schematic domain-walls structure (d).

because a and b are equal. A transition to the orthorhombic phase ($a \neq b$) is accompanied by rotation of cells in the neighbouring blocks. The rotation angle ε depends on the temperature which is illustrated by figure 10b. At twin boundary a particular structure occurs. Every Cu atom is surrounded by four O atoms. It is obvious that the boundary would influence the crystal's superconducting state. From an analysis of the Ginzburg-Landau equation it follows [44] that the wave function phase can jump at the twin boundary (Fig. 10c). All this results in a formation of domains with an irregular space distribution of the charge density. The crystallographic twin structure could induce a similar structure in the electronic subsystem. This is how a sequence of superconducting layers divided by normal conducting regions appears in a HTSC single crystal [45]. An illustration of such possibility is given by figure 10d. The normal conducting walls are metastable when $T < T_c$. Their existence depends on both the cooling rate and on the strength of the constant external magnetic field. An electron microscopy and structural studies indicate [46, 47] that the distance between walls is d = 500-1 000 Å while their thickness is about $\Delta d \approx 50$ Å. The normal walls do not influence the constant current flow along the superconducting domains. An arbitrary distribution of walls does not destroy the overall superconductivity of the material, but changes the critical current value [9, 45].

Concerning a microwave field the normal walls between the superconducting domains can be the source of the residual resistance.

The wall's contribution to the surface resistance is depend upon their orientation as regards to the incident electromagnetic wave polarization. If the **E** vector is orthogonal to the wall then to the expression (28) a term is added which corresponds to the wall resistance [48] :

$$R_w^{\perp} = \frac{1}{2}\frac{\Delta d}{d}(\lambda\sigma_2)^{-1}\{1 + [\omega\mu_0\lambda^2\sigma(t)]^2\}\ .$$

If **E** is collinear to the walls we have

$$R_w^{\parallel} = \frac{1}{2}\frac{\Delta d}{d}(\lambda\sigma_2)^{-1}(\omega\mu_0\lambda^2\sigma_2)^2\ .$$

Here, σ_2 is the temperature independent conductivity of the wall. For an arbitrary mutual orientation of the wall and **E** one can average over different contributions to the resistance :

$$R_s = \frac{R_0\,\Omega_0^2}{[f(t)]^{3/2}}\left\{\left(1 - \frac{\Delta d}{d}\right)t^{1/2} + A[\beta^2 + t + f(t)^2\,\Omega_0^{-2}]\right\}\ , \quad (30)$$

where

$$R_0 = [2\lambda(0)\sigma(1)]^{-1}\ , \quad \Omega_0 = \omega\mu_0\lambda^2(0)\sigma(1)\ ,$$

$$\sigma(1) = [\rho(1)]^{-1},$$

$$\beta = \frac{\sigma_2}{\sigma(1)}, \quad A = \frac{1}{2}\frac{\Delta d}{d}\beta^{-1}.$$

For $t \ll 1$, $t^{1/2} \gg t \gg t^{3/2}$, then all higher powers of t in previous expression can be omitted and we write :

$$R_s \cong R_0 \Omega_0^2 \left[A(\Omega_0^{-2} + \beta^2) + \left(1 - \frac{\Delta d}{d}\right) t^{1/2}\right].$$

Figure 11 shows R_s plotted as a function of $t^{1/2}$ which is more convenient for our purposes. This plot is calculated by expression (30) at 60 GHz, $\lambda(0) = 3 \times 10^{-7}$ m and $\rho(1) = 10^{-6}\ \Omega \times$ m. The curve 1 corresponds to $A = 0$ and the curve 2 to reasonable values of parameters : $\Delta d/d = 0{,}2$ and $\beta = 10$. The latter curve is in close agreement with experiment [23].

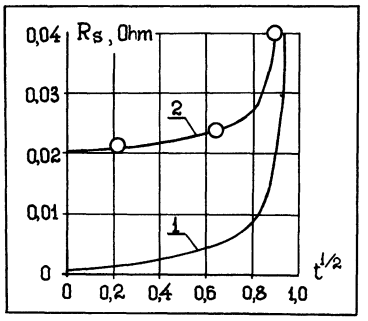

Fig. 11. — Temperature dependence of R_s ($R_{res} = 0$) (1), and with R_{rcs} taken into account by expression (30), (2). Experimental data are taken from [23].

Our suggestion concerning the contribution of the domains walls to the residual resistance needs and additional experimental investigation. Such an investigation must combine microscopic and structural studies of the domains with R_s measurements at different frequencies. The polarization of the incident electromagnetic wave and the constant magnetic field direction are also of great importance.

6. Conclusions.

The experimental data on the RF and microwave properties of HTSC materials obtained to this day enable us to suggest phenomenological models and to make reasonable predictions as to temperature and frequency dependences of such materials' parameters. One of the most interesting problems of the HTSC physics is the nature of the residual resistance. Once this problem is settled new ways would open to technological realizations of epitaxial films and single crystals with reduced residual resistance.

In the present review we passed over in silence the magnetic field influence on HTSC properties. This problem is intensively studied in dc regimes [49, 50]. The RF and microwave regime in the presence of magnetic field are now under study [16, 17, 45] which could give valuable information on the integranular junctions and/or twinned domains.

Acknowledgments.

The authors are very grateful to Prof. V. I. Safarov for initiating attention to this work.

References

[1] GOR'KOV L. P., KOPNIN N. B., *Usp. Fiz. Nauk* **156** (1988) 1, 117 (in Russian).

[2] HULM J. K., LAVERICK C., *Cryogenics* **28** (1988) 8, 545.

[3] LIKHAREV K. K., SEMENOV B. K., ZORIN A. B., In Itogi nauki i tekhniki VINITI AN SSSR, *series Superconductivity,* (Moscow) **1** (1988) in Russian.

[4] VENDIK O. G., GAÏDYKOV M. M., KOZYREV A. B., KOLESOV S. G., Proceedings of 18-th European Microwave Conference (Microwave Exhib. and Publish. Ltd.) 1988, p. 27.

[5] VENDIK O. G., KOZYREV A. B., Proceedings of 5-th International School on Microwave Physics and Technique (World Scientific) 1987, p. 231.

[6] MANKIEWICH P. M., SCOFIELD J. H., SKOCPOL W. S. *et al., Appl. Phys. Lett.* **51** (1987) 21, 1753.

[7] GOLOVASHKIN A. I., EKIMOV E. V., KRASNOSVOBODTSEV S. I., PECHEN E. V., *JETP Lett.* **47** (1988) 3, 191.

[8] STORMER H., LEVI A., BALDWIN K. *et al., Phys. Rev.* **B38** (1988) 4, 2472.

[9] MANNHART J., CHAUDHARI P., DIMOS D. *et al., Phys. Rev. Lett.* **61** (1988) 21, 2476.

[10] ALLEN L. H., BROUSARD P. R., CLAASEN J. H., WOLF S. A., *Appl. Phys. Lett.* **53** (1988) 14, 1338.

[11] SATO H., ZHU W., ISHIGURO T. J., *Solid State Chem.* **75** (1988) 2, 207.

[12] FACE D. E., NEAL M. J., MATTHIESSEN M. M., *et al., Appl. Phys. Lett.* **53** (1988) 3, 246.

[13] STATT B., WANG Z., LEE M. *et al., Physica C* **156** (1988) 2, 251.

[14] ADASHI H., WASA K., ICHIKAWA Y. *et al., J. Crystal Growth* **91** (1988) 3, 352.

[15] PARKIN S. S. P., LEE V. Y., NAZZEL A. I. *et al., Phys. Rev. Lett.* **61** (1988) 6, 750.

[16] VENDIK O. G., GAÏDUKOV M. M., GRABOY I. E. *et al., Pis'ma Zh. Tekh. Fiz.* **14** (1988) 21, 2001 (in Russian).

[17] FASTAMPA R., GIURA M., MARCON R., MATACOTTA C., *Europhys. Lett.* **6** (1988) 3, 265.
[18] PERSCIVAL T., THORN J., DRIVER R., *Electron. Lett.* **23** (1987) 23, 1125.
[19] ANSHUKOVA N. V., GOLOVASHKIN A. I., ZHURKIN B. G. *et al.*, Kratk. Soobshch. Fiz. AN SSSR Fiz. Inst. P. N. Lebedeva USSR (1988) 2, 32 (in Russian).
[20] SRIDHAR S., KENNEDY W., *Rev. Sci. Instrum.* **59** (1988) 4, 531.
[21] KLEIN N., MÜLLER G., PIEL H. *et al., Appl. Phys. Lett.* **54** (1989) 8, 757.
[22] ZACHPOULOS C., KENNEDY W. L., SRIDHAR S., *Appl. Phys. Lett.* **53** (1988) 25, 2168.
[23] VENDIK O. G., GAÏDUKOV M. M., GOLOVASHKIN A. I. *et al., Pis'ma Zh. Tekh. Fiz.* **14** (1988) 24, 2209 (in Russian).
[24] CARINI J., AWASTHI A., BETERMANN W. *et al., Phys. Rev.* **B37** (1988) 16, 9726.
[25] MARTENS J., BAYER J., GINSLEY D., *Appl. Phys. Lett.* **52** (1988) 21, 1822.
[26] BIELSKI M., VENDIK O. G., GAÏDUKOV M. M. *et al., JETP Lett.* **46** (1987) Suppl., 145.
[27] VARLASHKIN A. V., VASIL'EV A. L., GOLOVASHKIN A. I. *et al., JETP Lett.* **46** (1987) Suppl., 52.
[28] KENNEDY W. L., SRIDHAR S., *Solid State Comm.* **68** (1988) 1, 71.
[29] HYLTON T. L., KAPITULNIK A., BEASLEY M. R., *Appl. Phys. Lett.* **53** (1988) 4, 1343.
[30] VENDIK O. G., KOZYREV A. B., POPOV A. Yu., *Zh. Tekh. Fiz.* **59** (1989) 1, 107 (in Russian).
[31] LIKHAREV K. K., Introduction to Josephson junctions dynamics (Moscow, Nauka) 1985, (in Russian).
[32] KAUTZ R. L., *J. Res. NBS* **84** (1979) 1, 247.
[33] VENDIK O. G., *Pis'ma Zh. Tekh. Fiz.* **14** (1988) 12, 1098 (in Russian).
[34] ALEKSANDROV A. S., *JETP Lett.* **46** (1987) Suppl., 107.
[35] SCHRIEFFER J. R., WON X.-G., ZHANG S.-C., *Phys. Rev. Lett.* **60** (1988) 10, 944.
[36] LOH E., MARTIN J., PRELOVSEK P., CAMPBELL D., *Phys. Rev.* **B48** (1988) 4, 2494.
[37] HAZEN R. M., FINGER L. W., ANGEL R. J. *et al., Phys. Rev.* **B35** (1987) 13, 7238.
[38] COOPER J. R., CHU C. T., ZHOU L. W. *et al., Phys. Rev.* **B37** (1988) 1, 638.
[39] PROCH A., WOLDROM J., COHEN, *J. Phys. F. Met. Phys.* **18** (1988) 7, 1547.
[40] ALEKSANDROV A. S., TRAVEN' S. A., *Pis'ma Zh. Eksp. Teor. Fiz.* **48** (1988) 8, 426 (in Russian).
[41] WU M. K., ASHBURN J. R., TORN C. J. *et al., Phys. Rev. Lett.* **58** (1987) 9, 908.
[42] DI JORIO M., ANDERSON A., ISAUR B., *Phys. Rev.* **B38** (1988) 10, 7019.
[43] HODEAU J. L., CHAILLOUT C., CAPPONI J. J., MAREZIO M., Solid State Comm. **64** (1987) 11, 1349.
[44] ANDREEV A. F., *JETP Lett.* **46** (1987) 11, 584.
[45] GUREVICH A. Vl., MINTS V. G., *Pis'ma Zh. Eksp. Teor. Fiz.* **48** (1988) 4, 196 (in Russian).
[46] OSIP'JAN Yu. A., AFONIKOVA N. S., EMEL'CHENKO, G. A., *et al., Pis'ma Zh. Eksp. Teor. Fiz.* **46** (1987) 5, 189 (in Russian).
[47] GARCIA N., VIEIRA S., BARO A. M., *Z. Phys. B, Cond. Matter.* **70** (1988) 1, 9.
[48] VENDIK O. G., KOWALEWICH L., KOZYREV A. B. *et al., Pis'ma Zh. Tekh; Fiz.* **15** (1989) 8, 72 (in Russian).
[49] SONIN E. B., *Pis'ma Zh. Eksp. Teor. Fiz.* **47** (1988) 8, 415 (in Russian).
[50] TINKHAM M., *Phys. Rev. Lett.* **61** (1988) 14, 1658.